Femtosecond dynamics of the structural transition in mixed valence manganites

A. Caviezel,[1,*] U. Staub,[1] S. L. Johnson,[2] S. O. Mariager,[1] E. Möhr-Vorobeva,[1,†] G. Ingold,[1] C. J. Milne,[3] M. Garganourakis,[1] V. Scagnoli,[1] S. W. Huang,[1] Q. X. Jia,[4] S.-W. Cheong,[5] and P. Beaud[1]

[1]*Swiss Light Source, Paul Scherrer Institut, 5232 Villigen PSI, Switzerland*

[2]*Institute for Quantum Electronics, Physics Department, ETH Zurich, 8093 Zurich, Switzerland*

[3]*Laboratoire de Spectroscopie Ultrarapide, Ecole Polytechnique Fédérale de Lausanne, 1015 Lausanne, Switzerland*

[4]*Center for Integrated Nanotechnologies, Los Alamos National Laboratory, Los Alamos, New Mexico 87545, USA*

[5]*Rutgers Center for Emergent Materials and Department of Physics & Astronomy, Rutgers University, Piscataway, New Jersey 08854, USA*

(Received 15 August 2012; published 9 November 2012)

We investigate the structural response of charge and orbitally ordered (CO/OO) manganites to ultrafast optical excitation using optical reflectivity and x-ray diffraction as a probe. We study a $La_{0.42}Ca_{0.58}MnO_3$ (LCMO) thin film and a $La_{0.25}Pr_{0.375}Ca_{0.375}MnO_3$ (LPCMO) single crystal. For both materials we observe oscillations in the optical responses that are assigned to a coherent optical phonon generated via displacive excitation. The coherent phonon disappears either when increasing the temperature above $T_{CO/OO}$ or when raising the excitation fluence above a certain threshold. At low excitation fluences the amplitude and lifetime of this phonon behave similarly to the order parameter of the structural phase transition.

DOI: 10.1103/PhysRevB.86.174105 PACS number(s): 64.60.A−, 61.05.cp, 71.27.+a, 78.47.J−

I. INTRODUCTION

The exploration of material classes with rich phase diagrams and finding ways to control the individual phases have been subjects of continuing interest in materials science.[1–7] In many systems the change of the macroscopic properties is related to a rearrangement of the long-range electronic, magnetic, and atomic order. For the understanding of the underlying physical processes of the corresponding phase transitions experimental tools on relevant time scales are extremely helpful. X-ray diffraction and absorption with femtosecond time resolution are highly successful methods to directly study the dynamics of order parameters.[8–15] Furthermore, time-resolved optical spectroscopies employing ultrafast lasers are widely used to study materials even though they lack direct structural sensitivity. Sources of tunable ultrashort x-rays to gather direct structural information typically involve large scale facilities[16–20] where the available time for experiments is scarce and precious. Consequently, only a few studies have been performed up to date.

Perovskite manganites offer an almost infinite field to investigate the interaction of charge, structure, and spin. By far the best known manifestation of the interplay of these different degrees of freedom is the colossal magnetoresistance effect.[21] The material properties are not only susceptible to external conditions such as temperature, applied magnetic, or electric field, but also to chemical doping and photoexcitation.[1,2,22–26] The latter provides the opportunity to trigger electronic, vibrational, and magnetic excitations with ultrashort pulses ranging from visible to far infrared and to study the dynamical response with time-resolved optical[23,25,27–29] or diffraction techniques.[26,30–32] In this paper we compare a $La_{1-x}Ca_xMnO_3$ (LCMO) and $La_{5/8-y}Pr_yCa_{3/8}MnO_3$ (LPCMO) compound.

LCMO is one of the most studied compounds since the Ca^{2+} and La^{3+} ions match almost perfectly in size and therefore allows synthesis over the entire doping range.[33] The Mn valence varies from trivalent in $LaMnO_3$ to tetravalent in $CaMnO_3$ where the ionic size of Mn^{3+} is significantly larger compared to Mn^{4+}.[21] The octahedrally coordinated Mn^{3+} ions show a strong Jahn-Teller effect.[34] The hopping of the e_g electron between the two different valent Mn ions favors ferromagnetic coupling in the double exchange mechanism,[35] whereas the superexchange interaction favors an antiferromagnetic alignment of the spins. These competing interactions are responsible for the close interplay among charge carriers, orbitals, spins, and structural distortions in this mixed-valence manganite. For a hole doping of $x = 0.17$–0.5 the paramagnetic phase at room temperature changes at low temperatures into a ferromagnetic state via an insulator-metal transition, whereas for $x > 0.5$ the low temperature state remains insulating but with antiferromagnetic order.[36] For $x = 0.5$ the charge order leads to a doubling of the unit cell.[37] In addition, the orbital order distorts the oxygen octahedra due to the Jahn-Teller effect.[38]

LPCMO is an interesting material to study as it is close to the border between the FM metallic and AFM insulating state. Only a small magnetic field is required to switch between these phases.[1,39,40] Charge ordering occurs for $y \geqslant 0.3$ with $T_{CO} \sim 210$ K independent of y. The critical temperature T_C, however, is strongly reduced from 210 K (at $y = 0.25$) to 80 K for $y = 0.3$, indicating a strong competition between the dominant FM and CO phases in the ground state.[1]

Recently, femtosecond x-ray diffraction was used to directly probe the structural dynamics of a charge and orbitally ordered thin film of $La_{0.42}Ca_{0.58}MnO_3$.[26] It was shown that photoexcitation can induce an ultrafast phase transition as evidenced by the disappearance of a superlattice reflection. The change of structural symmetry occurs on a nonthermal time scale with initial dynamics significantly faster than the experimental time resolution of 200 fs (FWHM). Here we focus on using time-resolved optical reflectivity as a primary method to study the charge and orbitally ordered (CO/OO) phase and its behavior upon photoexcitation in a thin LCMO ($x = 0.58$) film and a single crystal of LPCMO ($y = 3/8$). We complement this study with results obtained by ultrafast x-ray diffraction experiments.

II. EXPERIMENT

The epitaxial (001)-oriented $La_{0.42}Ca_{0.58}MnO_3$ film with a thickness of 200 nm has been grown by pulsed laser deposition by a XeCl excimer laser ($\lambda = 308$ nm) on a double side polished (100) MgO substrate. The manganite film was deposited while the substrate is kept at a temperature of 825 °C under an oxygen pressure of 400 mTorr during the deposition. The $La_{0.25}Pr_{0.375}Ca_{0.375}MnO_3$ single crystal has been grown in an optical floating-zone furnace[41] and is cut and polished to a (001) surface orientation. Throughout this paper we use the orthorhombic lattice indices of the room temperature unit cell notation which has $Pbnm$ symmetry.[37]

Optical femtosecond time-resolved reflectivity measurements were carried out with a 2 kHz Ti:sapphire laser system delivering 50 fs pulses at a wavelength of 800 nm. In this experiment a closed cycle refrigerator (Janis RDK-205D) with a Sumitomo compressor (CNA-11C) was used to obtain temperatures down to 4 K. A cross polarized single color setup between the pump and probe beam was chosen to eliminate interferences at time zero. A polarizer in front of the 5×5 mm^2 silicon detector (DET36A) prevents scattered light from the stronger pump pulse to be detected with the weaker probe pulse. The voltage output of the photodiode was integrated using a Boxcar integrator. The data acquisition system is described elsewhere[42] and has been used for the laser experiments as well as for the time-resolved x-ray experiments. The pump beam was chopped at 1 kHz to measure the excited as well as the unexcited response alternately and the reflectivity change signal $\Delta R/R$ was extracted shot-by-shot. This way slow drifts in the electronics and detectors are eliminated. The time resolution was measured separately by cross correlation of the pump and probe pulses in a 0.2-mm-thick BBO crystal.

For the x-ray measurements we used a fragment of the same LPCMO crystal but cut and polished to (010) orientation. Static x-ray diffraction measurements were performed at the Material Science Beamline (X04SA) at the Swiss Light Source (SLS). The sample was cooled with a cryogenic chamber or a liquid nitrogen jet. The reflected intensities of the Bragg peak were recorded with a 2D PILATUS II pixel detector.[43]

Time-resolved hard x-ray diffraction measurements were performed at the FEMTO slicing beamline at the SLS[18] employing a grazing incidence geometry.[44,45] For the LCMO experiment the x-ray energy was set to 7.1 keV. Choosing an incident angle of 0.7° allows matching the x-ray probe depth (∼55 nm) to the very short absorption length of the optical pump of 65 ± 5 nm estimated from optical conductivity data.[46] Additionally the larger acceptance angles at grazing incidence allow us to make more efficient use of the low photon flux (250 photons/pulse at 2 kHz) and intrinsically large bandwidth due the single Mo/B_4C-multilayer monochromator with 1.2% bandwidth. The hexapod sample manipulator enters via a rotary vacuum feedthrough into a vacuum chamber equipped with a large Kapton window enabling the diffracted x-rays to exit the chamber. The sample is mounted on a copper block whose temperature can be stabilized between 35 and 300 K. We excite the sample with a weakly focused (450×560 μm^2) 100 fs laser pulse with π-polarization incident at 1 kHz at a grazing angle of 10°. The x-ray probe beam is strongly focused vertically to a size less than 250×10 μm^2. For the LPCMO experiment the x-ray incident angle was 0.85° and the energy was set to 5.0 keV, which is below the Mn K and Pr L edges to minimize fluorescence resulting in a x-ray probe depth of 90 nm. The temporal resolution of 200 ± 20 fs (FWHM) and the coincidence time t_0 between the optical pump and x-ray probe pulses were independently determined by measuring the well characterized coherent optical A_{1g} phonon in bismuth.[44]

III. RESULTS

A. Optical results

Time-resolved pump-probe reflectivity transients versus temperature for LCMO at an incident pump fluence $F = 0.37$ mJ/cm^2 and for LPCMO at $F = 3.0$ mJ/cm^2 are shown in Figs. 1(a) and 1(b), respectively. The LCMO data are very similar to those obtained at much lower pump fluences: A laser-induced coherent oscillation with a period of approximately 500 fs that is present in the charge ordered phase ($T \leqslant T_{CO} \approx 225$ K).[23] We observe a somewhat lower frequency of 2.05 ± 0.1 THz in our experiment compared to the 2.2 THz found by Lim *et al.*[23] This is most likely due to a softening of the interatomic potential from strong excitation of the electronic system, similar to that observed in bismuth and related materials.[44,47] The LPCMO crystal shows similar behavior as the LCMO film. The coherent oscillation with a frequency of 2.5 THz disappears when heated over $T_{CO} \approx 210$ K. This is in accordance with the findings of Jang *et al.*[48] measured with a pump fluence of 0.1 mJ/cm^2.

Figure 2 shows the reflectivity changes measured at 60 K with laser fluences ranging from 0.5 to 7.7 mJ/cm^2 for LCMO and 1.0 to 14.0 mJ/cm^2 for LPCMO. Such data sets were recorded at 5, 60, 100, 140, 180, 220, and 260 K. For the LCMO sample, the amplitude of the observed coherent phonon

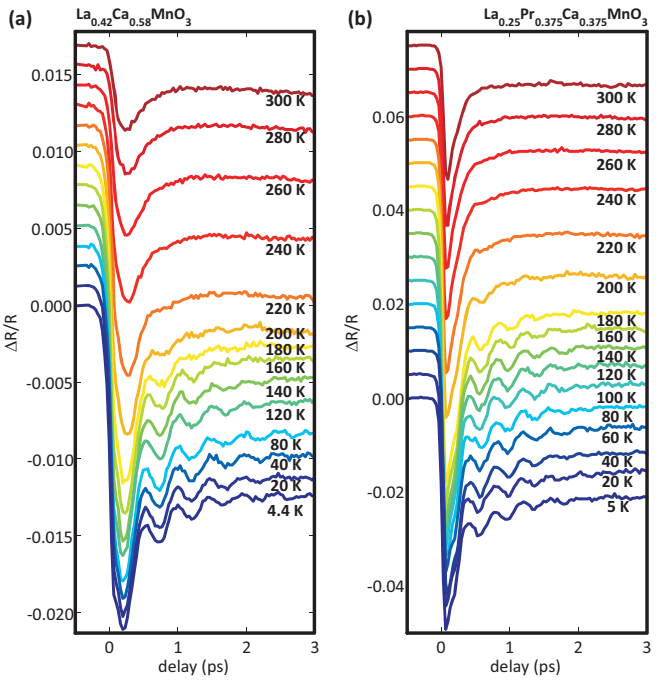

FIG. 1. (Color online) Temperature dependence of the temporal response of the optical reflectivity. (a) LCMO at incident fluence $F = 0.37$ mJ/cm^2, and (b) LPCMO at $F = 3.0$ mJ/cm^2.

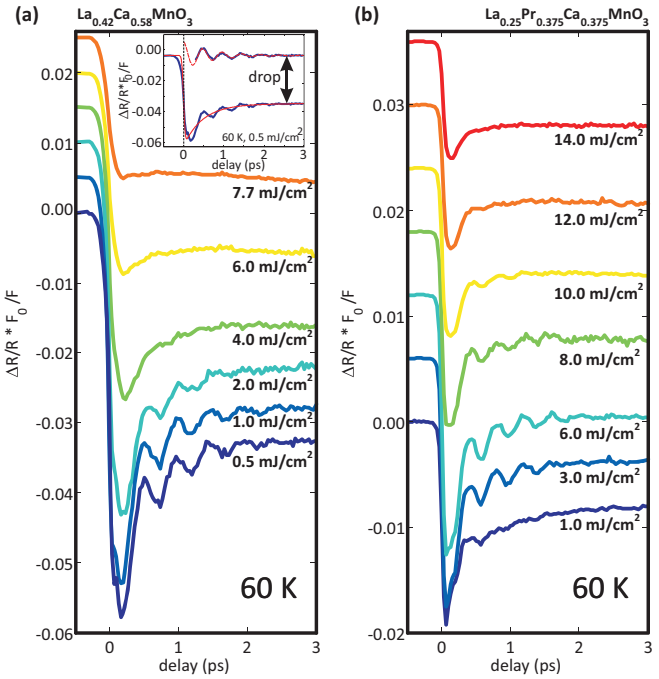

FIG. 2. (Color online) Normalized excitation fluence dependence of the temporal response of the optical reflectivity at 60 K ($F_0 = 1.0$ mJ/cm^2) for (a) LCMO and (b) LPCMO, respectively. Inset: Lower curve: Time trace fitted with a double exponential for the incoherent electronic response. Upper curve: Remaining oscillatory response after subtraction of the fitted incoherent response with its cosine fit.

increases linearly with fluence until it starts to saturate at about 1.5 mJ/cm^2 and eventually disappears at the highest fluences (>4 mJ/cm^2). We do not observe any noticeable damage or indications of permanent CO/OO melting. For the LPCMO crystal we find that the phonon amplitude is hardly discernible at low fluence. It increases nonlinearly up to a fluence of approximately 6 mJ/cm^2 before it also starts to saturate. The overall pump induced change $\Delta R/R$ reached after 3–4 ps increases linearly with fluence for both samples up to a fluence of about 4 and 10 mJ/cm^2 for LCMO and LPCMO, respectively. Such data sets were recorded for both samples for a set of temperatures between 5 and 260 K. We find qualitatively similar behavior at all temperatures but the fluence needed to suppress the phonon and to saturate the change in $\Delta R/R$ decreases when approaching T_{CO}. The nonlinear behavior of the phonon amplitude for LPCMO at low fluences below 3 mJ/cm^2 is only observed at a temperature below 140 K.

B. X-ray results

The structural distortion associated with the CO/OO leads to weak superstructure reflections for both samples. For LPCMO we find $q/b^* = 1/2$, where b^* is the reciprocal lattice vector. This corresponds to the expected CE-type charge and orbital order.[38] The temperature dependence of a superlattice reflection is shown in Fig. 3 for both the LCMO film and the LPCMO crystal. The transition temperatures for the LCMO and the LPCMO samples are in agreement with previously published values of 225 and 210 K, respectively.[1,49] Whereas

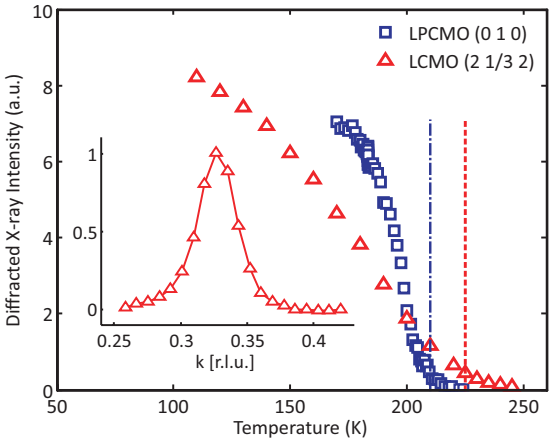

FIG. 3. (Color online) Temperature dependence of the superlattice reflections (2 1/3 2) of the LCMO film and (0 1 0) of the LPCMO single crystal. Note: The (010) peak is similarly sensitive to the low temperature distortion since it is forbidden in $Pbnm$ notation. The dashed-dotted and the dotted line mark transition temperatures T_{CO} taken from literature for LPCMO[1] and LCMO,[49] respectively. Inset: Reciprocal space k scan for LCMO at 100 K from which the diffracted intensity is extracted.

the superlattice reflection of the LPCMO reflects a doubling of the high-temperature unit cell, the LCMO cell triples, due to the slightly higher Ca content of $x = 0.58$ which is consistent with the results on bulk LCMO.[50] This can be nicely seen from the reciprocal space scan shown in the inset of Fig. 3.

Figure 4(a) shows the temporal evolution of the $(5 - 2^2/_3\ 2)$ superlattice reflection measured at 150 K for several pump fluences. These data are very similar to those of Ref. 26 using a thinner 50 nm film with nominally the same composition. At

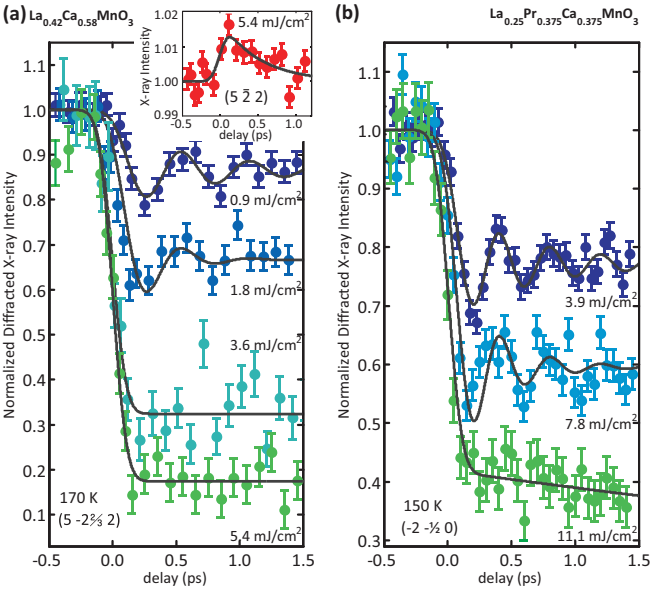

FIG. 4. (Color online) (a) Time traces of the diffracted intensity of the LCMO $(5 - 2^2/_3\ 2)$ superlattice peak for LCMO at different excitation fluences. Inset: Response of the regular $(5\ {-2}\ 2)$ reflection for an absorbed fluence of 5.4 mJ/cm^2. (b) Time traces of the diffracted intensity of the LPCMO $(-2\ -^1/_2\ 0)$ superlattice reflection.

low excitation fluences we observe the displacive excitation of the coherent optical A_g phonon also seen in the optical transients. At high fluence the measured $(5\ -\ 2^2/_3\ 2)$ superlattice reflection drops by approximately 80% on the time scale of the experimental time resolution of 200 fs (FWHM). This initial nonthermal step of the phase transition has been attributed to the motion of the Mn^{4+} atoms along the $Pbnm$ x direction caused by the release of the Jahn-Teller distortion at the Mn^{3+} sites.[26] We also measured the dynamics of the regular $(5\bar{2}2)$ Bragg reflection, which for this phase transition should increase by approximately 5% estimated by structure factor calculations. The measurement [inset in Fig. 4(a)] shows a prompt 1.5% increase followed by a slow decay which is due to the onset of laser induced lattice disorder. The laser induced response of the $(-2\ -^1/_2\ 0)$ superlattice reflection of LPCMO is shown in Fig. 4(b). It exhibits a similar behavior as for LCMO but a larger fluence is required to suppress the phonon and to initiate the structural phase transition.

IV. DISCUSSION

A common feature of the transients in Fig. 1 is that following excitation at $t = 0$ a time resolution limited drop in $\Delta R/R$ is observed. This drop reflects the change of the optical permittivity caused by hot electrons. Subsequently the electron system relaxes quickly via electron-electron and electron-phonon scattering to a longer lived state. On top of this the oscillation in $\Delta R/R$ caused by the coherent optical phonon is clearly visible. In order to systematically extract the relative phonon amplitude and lifetime we follow the procedure that is illustrated in the inset of Fig. 2 showing the LCMO transient recorded at 60 K and 0.5 mJ/cm^2. First the transient is fitted by a double exponential and the result subtracted from the data. The remaining cosinelike oscillation, as seen from the fit to the oscillatory part in the inset of Fig. 2, is clear evidence that the generation mechanism of the phonon is of displacive character. In contrast, an impulsive nonresonant Raman excitation would lead to a phase shift of $\pi/2$ in the oscillation.[51] We extract the relative phonon amplitude for all data sets using the Fast Fourier transformation technique. Figure 5(a) shows the Fourier transform of the isolated oscillating part for the LCMO data shown in Fig. 1(a). It reveals a rather stiff frequency behavior versus temperature, that is, there is almost no softening of the mode. The same is true for the 2.5 THz phonon of the LPCMO sample. The temperature dependence of the phonon amplitudes and lifetimes for both samples are shown in Figs. 5(b) and 5(c), respectively. They both behave like an order parameter of the CO/OO phase.

We also plot the temperature dependence of the relative phonon amplitude for LPCMO measured at 1 mJ/cm^2. Clearly the material response is significantly different at this fluence for temperatures of 100 K and below. The temperature dependence seems to indicate that these observations may be related to the ferromagnetic phase ($T_C \approx 80$ K).[24] These complex dynamics are currently the subject of further studies. Here we are concentrating on the dynamics related to the melting of the charge and orbital ordered phase.

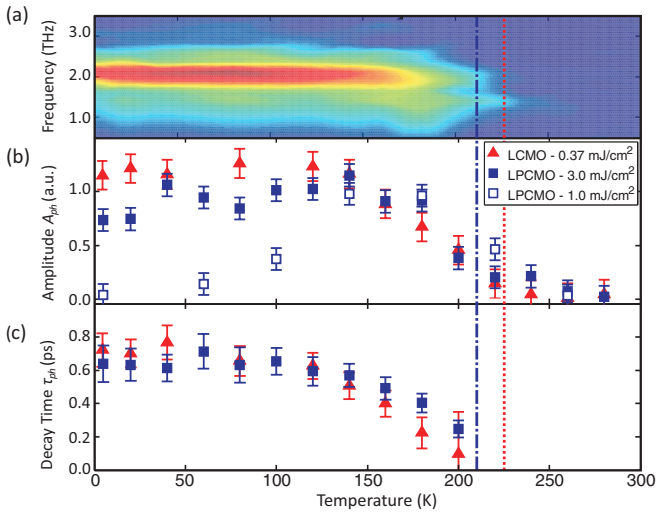

FIG. 5. (Color online) (a) Fourier transform of the coherent response of the optical pump-probe transients for LCMO for a pump fluence of 0.37 mJ/cm^2. (b) Extracted phonon amplitude A_{ph} and (c) phonon decay time τ_{ph} as a function of temperature. The dashed-dotted and the dotted line mark T_{CO} for LPCMO and LCMO, respectively.

As previously mentioned, when approaching the phase transition by heating the sample both the phonon amplitude and lifetime start to decrease. The same behavior is found upon increasing the fluence of the exciting laser pulse toward a certain threshold. The fluence dependence of the phonon amplitudes are shown in Fig. 6. For LPCMO [see Fig. 6(b)] the reduced amplitude observed at low fluences and low temperatures is clearly visible. However, at higher temperatures and fluences the normalized phonon amplitudes decrease linearly with fluence as they do for LCMO over the whole range measured. We define the suppression fluence F_{sup} as the zero crossing determined from a linear fit to the data. We also note that the steady-state level in the measured $\Delta R/R$ drops proportionally to the laser fluence. The size of this drop increases linearly with fluence until approaching a saturation fluence F_{sat}. Upon further increasing the pump fluence the size of this drop remains constant. F_{sat} is determined by the intersection of the linear increase at low fluences and the saturation plateau [see inset of Fig. 7]. As shown in Fig. 7 we find close agreement between F_{sat} and the values obtained for F_{sup} and we will discuss in the following that these fluences coincide with the threshold fluence for melting the CO/OO derived from x-ray diffraction experiments.

The temporal evolution of the normalized diffracted x-ray intensities of the superlattice peaks [see Fig. 4] are fitted for times $t > 0$ with

$$I(t)/I_0 = 1 - A[1 - e^{-t/\tau_1}\cos(2\pi f t)] - (1 - A)(1 - e^{-t/\tau_2}), \quad (1)$$

where $I_0 = I(t < 0)$. The first term on the right-hand side of Eq. (1) describes a displacively excited coherent optical phonon[52] where A is the phonon amplitude, f is its frequency, and τ_1 is its lifetime. The second term describes a further exponential decay of the superlattice peak intensity to fully complete the structural phase transition on a longer time τ_2.

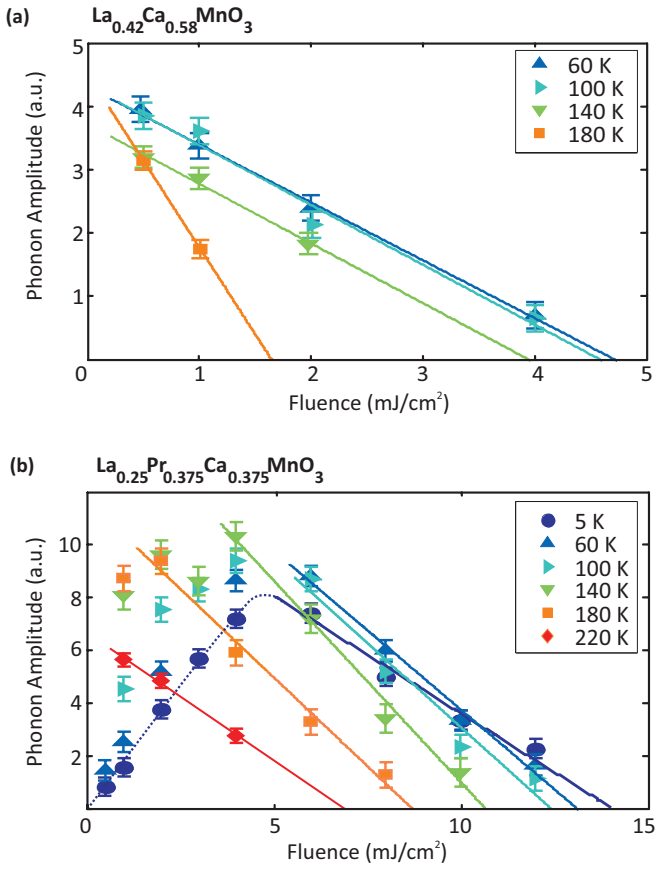

FIG. 6. (Color online) Fluence dependence of the phonon amplitude in optical pump-probe transients for (a) LCMO and (b) LPCMO, respectively. The zero crossing of the linear fit marks the suppression fluence F_{sup} needed to destroy the CO/OO. The dotted line in (b) indicates the increasing phonon amplitude with rising fluence for low temperatures in LPCMO.

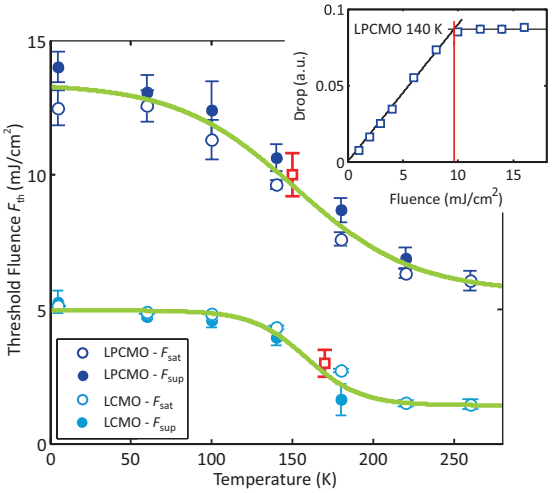

FIG. 7. (Color online) Threshold fluences for melting the CO/OO for LCMO and LPCMO evaluated by the decrease of the phonon amplitude A_{ph} (solid circles) and the saturation of the reflectivity level (open circles). The solid line is a guide to the eye. The inset displays the drop of the reflectivity level as a function of fluence for LPCMO at 140 K and the saturation fluence assignment. The threshold values extracted from the x-ray measurements are shown as squares.

The temporal resolution of 200 fs (FWHM) of the slicing source is taken into account by a convolution with a Gaussian of corresponding width. The fits are included in Fig. 4 as solid lines. The resulting phonon frequencies are 1.85 ± 0.1 THz for LCMO and 2.51 ± 0.12 THz for LPCMO, respectively. At the highest fluences the phonon becomes overdamped and the oscillations disappear in the fit.

However, after this initial drop the superlattice reflection is still present demonstrating that the change of lattice symmetry does not occur instantaneously as one could imply from the disappearance of the optical phonon in the optical data as recently concluded in an optical study on the insulator-to-metal transition in VO_2.[53] For LCMO it was shown that the change of lattice symmetry takes place within less than 50 ps at a pump fluence of 4.4 mJ/cm^2 as evidenced by the complete disappearance of the superlattice peak. And only after increasing the fluence above 7 mJ/cm^2 the complete change of structural symmetry occurs within approximately 1 ps.[26] In Fig. 4 the slower decay with time constant $\tau_2 = 14 \pm 8$ ps is clearly visible only for the LPCMO data taken at a fluence of 11.1 mJ/cm^2. We define the threshold fluence for melting the CO/OO as the fluence needed to saturate the first initial intensity drop which goes hand in hand with the suppression of the coherent oscillations. The thresholds are estimated to be 3 and 10 mJ/cm^2 for LCMO and LPCMO, respectively, and included as red squares in Fig. 7 agreeing well with the threshold values extracted from the optical data.

The microscopic picture for intense photodoping is the following. Photons with an energy of 1.55 eV mainly excite the intra-atomic $t_{2g}^3 e_g^1(\mathrm{Mn}^{3+}) \rightarrow t_{2g}^2 e_g^2(\mathrm{Mn}^{3+})$ transition. This filling of e_g states will instantaneously introduce local disorder to the orbital order. Subsequently the Jahn-Teller distortion of the Mn^{3+} oxygen octahedra is released followed by the ultrafast nonthermal structural phase transition.[26] The initial atomic motion occurring in this laser triggered transition must be those related to the rearrangement of the oxygen octahedra at the Mn^{3+} sites. These motions of the oxygen atoms are relatively small and will contribute only little to the overall change of diffraction intensity. In addition, the Jahn-Teller modes governing this process with frequencies in the order of approximately 14 THz[25] are significantly faster than our time resolution.

Comparing the low temperature $P2_1/m$ with the room temperature $Pbnm$ structure of LCMO ($x = 0.5$)[37] the major atomic motions occurring in this structural transition are motions along the crystal x direction of the $Mn^{4+}O_6$ sites by $dx_1 = 12$ pm and of the rare earth ions by $dx_2 = 5.6$ pm. These motions are indicated by arrows in Fig. 8(a). Since the collapse of the Jahn-Teller distortion at Mn^{3+} sites directly affects the Mn^{3+}-O-Mn^{4+} bond distances and angles, we conclude that the translational motion of the $Mn^{4+}O_6$ will take place earlier than that of the rare earth cations that occupy the empty spaces between the MnO_6 octahedra. We therefore tend to assign the observed coherent optical phonon to the x motion of the $Mn^{4+}O_6$ sites. At lower fluences the CO/OO is reduced, triggering the translational motion of the $Mn^{4+}O_6$

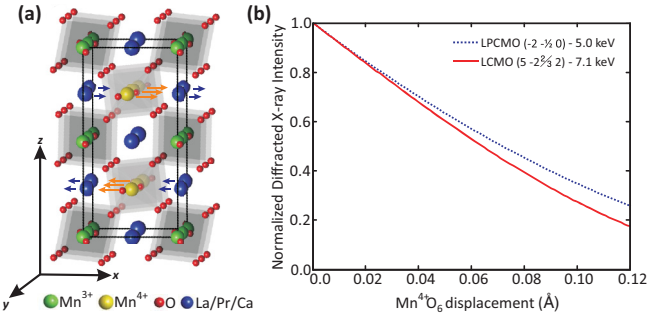

FIG. 8. (Color online) (a) Low temperature unit cell (solid lines) of a half-doped manganite using the atomic structure from Ref. 37. Arrows indicate the atomic motions in direction of the x axis of the $Mn^{4+}O_6$ and the La/Pr/Ca ions. (b) Calculated Bragg peak intensities with respect to the $Mn^{4+}O_6$ motion along the x axis.

sites. The linearity of the drop in the optical as well as in the x-ray data suggests that the distortion due to the long range OO continuously weakens with fluence. Once the threshold fluence to completely melt the CO/OO phase is reached the Mn^{4+} sites move to their new equilibrium positions on a time scale of less than 200 fs. Since the oscillations are not observed above F_{th} we must conclude that this motion becomes critically damped or overdamped. The time scale of the $Mn^{4+}O_6$ displacement is then expected to approach ~125 fs, that is, a quarter period of the optical phonon.[54] To complete the phase transition the rare earth cations must move to their new equilibrium position that occurs on the slower time scale τ_2. Note that the assignment of the coherent phonon is different than in a previous study[26] where it was attributed to the motion of the La/Ca sublattice based on an oxygen isotope Raman study on LCMO ($x = 0.3$).[55] However, the fact that we measure a higher frequency of the coherent phonon for LPCMO than for LCMO is inconsistent with the 25% mass increase of the La/Pr/Ca sublattice and favors the current assignment.

Using the constrained low temperature $P2_1/m$ structure (Table II in Ref. 37) we can calculate the dependence of the Bragg peak intensities on the motion of the Mn^{4+} sites along the coordinate dx_1. The result is shown for both samples in Fig. 8(b). Once the Mn^{4+} octahedra have moved to the position expected for the room temperature phase the calculation yields a drop of intensity of 83% for the LCMO ($5\ -2^1/_2\ 2$) and 74% for the LPCMO ($-2\ -^1/_2\ 0$) reflection. This is in excellent agreement with the diffracted intensity change $A = 0.83(5)$ obtained from the fit to the 5.4 mJ/cm^2 LCMO transient shown in Fig. 4(a). For the 11.1 mJ/cm^2 LPCMO transient we obtain $A = 0.58(3)$ which is lower than estimated but can be explained by the mismatch of the x-ray probe depth to the laser absorption length in the LPCMO experiment: Regions in the material that are less excited contribute significantly to the measured diffracted intensity.

The temperature dependence of the threshold fluences behaves like an order parameter of the charge and orbital order ground state. At a closer look, however, we find significant differences in the dynamical response of the two materials. The phonon frequency is lower for LCMO than for LPCMO and the threshold fluence for melting the CO/OO phase is significantly higher for LPCMO. The excitation densities at the threshold averaged over the laser absorption length accounts for the absorption of 3.6 and 1.4 photons per unit cell for LPCMO and LCMO, respectively. Hence the CO/OO phase in LPCMO is significantly more stable against photodoping than in LCMO. At first hand this is not expected, since in $(La_{1-y}Pr_y)_{1-x}Ca_xMnO_3$ low magnetic fields of about 1 T are sufficient to cause a large change in the conductivity indicating that the material lies on the bridge to the metal-insulator transition. However, changing the doping does not create a metallic state. This is in contrast to $La_{1-x}Ca_xMnO_3$, where the material becomes metallic when increasing the number of e_g electrons. Therefore our results suggest that the different threshold fluences reflect the different chemical doping behavior of these two compounds.

Accounting for the stoichiometric composition of the two compounds the density of photoexcited Mn^{3+} ions results in 70% and 40% for LPCMO and LCMO, respectively. Thus the difference between the number of excited $Mn^{3+}O_6$ units is less significant. This might indicate that the instant destruction of the orbital order by the interatomic Mn^{3+} transition is indeed the main driving mechanism for the laser-induced transition observed in many manganites on an ultrafast nonthermal time scale.

V. CONCLUSIONS

We have studied the dynamics of laser excited LCMO and LPCMO with time-resolved optical reflectometry over a wide range of temperatures and fluences. The amplitudes of the coherent optical phonons of A_g symmetry observed at low laser fluence are correlated with the underlying CO/OO phase. The observed disappearance of the phonon when raising the excitation fluence above a certain threshold is a good indicator of the onset of a structural phase transition. The loss of the equilibrium-phase phonon modes occurs promptly, indicating a nonthermal pathway for the photoinduced phase transition. But as the x-ray results show it does not imply an immediate change of lattice symmetry. The threshold fluences derived from the optical data are in excellent agreement with those directly measured using time-resolved x-ray diffraction. Although both materials studied behave qualitatively similarly, we find that the CO/OO phase in LPCMO is significantly more robust than in LCMO. The structural phase transition is a direct consequence of melting the charge and orbitally ordered phase. Consequently, the temperature dependence of the threshold fluences behaves like an order parameter of the phase transition. The x-ray data indicate that the ultrafast atomic displacement launching the coherent optical phonon continuously increases with fluence. We assign the motion of this phonon to that of the $Mn^{4+}O_6$ octahedra. This motion is a direct consequence of photodoping the Mn^{3+} sites that generates disorder in the orbital order created by propelling a Mn^{3+} electron from the t_{2g} to the e_g band and the subsequent collapse of the Jahn-Teller distortion at the $Mn^{3+}O_6$ sites. One possible way to substantiate the proposed assignment of the low frequency A_g phonon observed in CO/OO manganites is using time-resolved x-ray diffraction to measure and compare the phonon amplitude on several Bragg reflections with different sensitivities to the underlying atomic motion.

ACKNOWLEDGMENTS

We thank the Swiss National Science Foundation for financial support (Grant 200021_124496) and its National Centers of Competences in Research MUST and MaNEP. We are grateful to the microXAS beamline scientists Daniel Grolimund and Camelia Borca and Material Science beamline scientist Philip Willmott whose efforts have made these experiments possible. The work at Los Alamos was supported by the U.S. Department of Energy through the LANL/LDRD program and the Center for Integrated Nanotechnologies. S.W.C. acknowledges support from NSF (DMR-1104484).

*andrin.caviezel@psi.ch

†Present address: Department of Physics, Clarendon Laboratory, University of Oxford, Parks Road, Oxford OX1 3PU, United Kingdom.

[1] M. Uehara, S. Mori, C. H. Chen, and S.-W. Cheong, Nature (London) **399**, 560 (1999).

[2] M. Fiebig, K. Miyano, Y. Tomioka, and Y. Tokura, Appl. Phys. B **71**, 211 (2000).

[3] M. Rini, R. Tobey, N. Dean, J. Itatani, Y. Tomioka, Y. Tokura, R. W. Schoenlein, and A. Cavalleri, Nature (London) **449**, 72 (2007).

[4] T. Z. Ward, X. G. Zhang, L. F. Yin, X. Q. Zhang, M. Liu, P. C. Snijders, S. Jesse, E. W. Plummer, Z. H. Cheng, E. Dagotto, and J. Shen, Phys. Rev. Lett. **102**, 087201 (2009).

[5] D. Fausti, R. I. Tobey, N. Dean, S. Kaiser, A. Dienst, M. C. Hoffmann, S. Pyon, T. Takayama, H. Takagi, and A. Cavalleri, Science **331**, 189 (2011).

[6] A. Dienst, M. C. Hoffmann, D. Fausti, J. C. Petersen, S. Pyon, T. Takayama, H. Takagi, and A. Cavalleri, Nat. Photon. **5**, 485 (2011).

[7] T. Kampfrath, A. Sell, G. Klatt, A. Pashkin, S. Mährlein, T. Dekorsy, M. Wolf, M. Fiebig, A. Leitenstorfer, and R. Huber, Nat. Photon. **5**, 31 (2011).

[8] K. Sokolowski-Tinten, C. Blome, J. Blums, A. Cavalleri, C. Dietrich, A. Tarasevitch, I. Uschmann, E. Förster, M. Kammler, M. H. von Hoegen, and D. von der Linde, Nature (London) **422**, 287 (2003).

[9] M. Bargheer, N. Zhavoronkov, Y. Gritsai, J. C. Woo, D. S. Kim, M. Woerner, and T. Elsaesser, Science **306**, 1771 (2004).

[10] A. Cavalleri, M. Rini, H. H. W. Chong, S. Fourmaux, T. E. Glover, P. A. Heimann, J. C. Kieffer, and R. W. Schoenlein, Phys. Rev. Lett. **95**, 067405 (2005).

[11] A. Cavalleri, S. Wall, C. Simpson, E. Statz, D. W. Ward, K. A. Nelson, M. Rini, and R. W. Schoenlein, Nature (London) **442**, 664 (2006).

[12] E. Möhr-Vorobeva, S. L. Johnson, P. Beaud, U. Staub, R. De Souza, C. Milne, G. Ingold, J. Demsar, H. Schaefer, and A. Titov, Phys. Rev. Lett. **107**, 036403 (2011).

[13] C. Boeglin, E. Beaurepaire, V. Halt, V. López-Flores, C. Stamm, N. Pontius, H. A. Dürr, and J.-Y. Bigot, Nature (London) **465**, 458 (2010).

[14] S. O. Mariager, F. Pressacco, G. Ingold, A. Caviezel, E. Möhr-Vorobeva, P. Beaud, S. L. Johnson, C. J. Milne, E. Mancini, S. Moyerman, E. E. Fullerton, R. Feidenhans'l, C. H. Back, and C. Quitmann, Phys. Rev. Lett. **108**, 087201 (2012).

[15] S. L. Johnson *et al.*, Phys. Rev. Lett. **108**, 037203 (2012).

[16] R. W. Schoenlein, S. Chattopadhyay, H. H. W. Chong, T. E. Glover, P. A. Heimann, C. V. Shank, A. A. Zholents, and M. S. Zolotorev, Science **287**, 2237 (2000).

[17] S. Khan, K. Holldack, T. Kachel, R. Mitzner, and T. Quast, Phys. Rev. Lett. **97**, 074801 (2006).

[18] P. Beaud, S. L. Johnson, A. Streun, R. Abela, D. Abramsohn, D. Grolimund, F. Krasniqi, T. Schmidt, V. Schlott, and G. Ingold, Phys. Rev. Lett. **99**, 174801 (2007).

[19] W. Ackermann *et al.*, Nat. Photon. **1**, 336 (2007).

[20] P. Emma *et al.*, Nat. Photon. **4**, 641 (2010).

[21] G. H. Jonker and J. H. V. Santen, Physica **16**, 337 (1950).

[22] O. V. Misochko, E. M. Kaidashev, N. Georgiev, T. Dekorsy, and I. N. Zakharchenko, JETP **97**, 788 (2003).

[23] D. Lim, V. K. Thorsmølle, R. D. Averitt, Q. X. Jia, K. H. Ahn, M. J. Graf, S. A. Trugman, and A. J. Taylor, Phys. Rev. B **71**, 134403 (2005).

[24] W. Wu, C. Israel, N. Hur, S. Park, S.-W. Cheong, and A. de Lozanne, Nat. Mater. **5**, 881 (2006).

[25] D. Polli, M. Rini, S. Wall, R. W. Schoenlein, Y. Tomioka, Y. Tokura, G. Cerullo, and A. Cavalleri, Nat. Mater. **6**, 643 (2007).

[26] P. Beaud, S. L. Johnson, E. Vorobeva, U. Staub, R. A. De Souza, C. J. Milne, Q. X. Jia, and G. Ingold, Phys. Rev. Lett. **103**, 155702 (2009).

[27] T. Ogasawara, M. Matsubara, Y. Tomioka, M. Kuwata-Gonokami, H. Okamoto, and Y. Tokura, Phys. Rev. B **68**, 180407 (2003).

[28] M. Matsubara, Y. Okimoto, T. Ogasawara, Y. Tomioka, H. Okamoto, and Y. Tokura, Phys. Rev. Lett. **99**, 207401 (2007).

[29] M. Först, C. Manzoni, S. Kaiser, Y. Tomioka, Y. Tokura, R. Merlin, and A. Cavalleri, Nat. Phys. **7**, 854 (2011).

[30] H. Ehrke, R. I. Tobey, S. Wall, S. A. Cavill, M. Först, V. Khanna, T. Garl, N. Stojanovic, D. Prabhakaran, A. T. Boothroyd, M. Gensch, A. Mirone, P. Reutler, A. Revcolevschi, S. S. Dhesi, and A. Cavalleri, Phys. Rev. Lett. **106**, 217401 (2011).

[31] M. Först, R. I. Tobey, S. Wall, H. Bromberger, V. Khanna, A. L. Cavalieri, Y.-D. Chuang, W. S. Lee, R. Moore, W. F. Schlotter, J. J. Turner, O. Krupin, M. Trigo, H. Zheng, J. F. Mitchell, S. S. Dhesi, J. P. Hill, and A. Cavalleri, Phys. Rev. B **84**, 241104 (2011).

[32] H. Ichikawa, S. Nozawa, T. Sato, A. Tomita, K. Ichiyanagi, M. Chollet, L. Guerin, N. Dean, A. Cavalleri, S.-I. Adachi, T.-H. Arima, H. Sawa, Y. Ogimoto, M. Nakamura, R. Tamaki, K. Miyano, and S.-Y. Koshihara, Nat. Mater. **10**, 101 (2011).

[33] E. Dagotto, *Nanoscale Phase Separation and Colossal Magnetoresistance: The Physics of Manganites and Related Compounds* (Springer, Berlin, 2003), p. 456.

[34] D. Reinen and C. Friebel, *Structural Problems* (Springer, Berlin, 1979), Vol. 37.

[35] C. Zener, Phys. Rev. **82**, 403 (1951).

[36] S.-W. Cheong and H. Hwang, *Ferromagnetism vs Charge/Orbital Ordering in Mixed-Valent Manganites*, edited by Y. Tokura (Gordon & Breach, London, 1999).

[37] E. E. Rodriguez, T. Proffen, A. Llobet, J. J. Rhyne, and J. F. Mitchell, Phys. Rev. B **71**, 104430 (2005).

[38]Y. Tokura and N. Nagaosa, Science **288**, 462 (2000).
[39]L. Ghivelder and F. Parisi, Phys. Rev. B **71**, 184425 (2005).
[40]P. A. Sharma, S. B. Kim, T. Y. Koo, S. Guha, and S.-W. Cheong, Phys. Rev. B **71**, 224416 (2005).
[41]H. J. Lee, K. H. Kim, M. W. Kim, T. W. Noh, B. G. Kim, T. Y. Koo, S.-W. Cheong, Y. J. Wang, and X. Wei, Phys. Rev. B **65**, 115118 (2002).
[42]M. Saes, F. van Mourik, W. Gawelda, M. Kaiser, M. Chergui, C. Bressler, D. Grolimund, R. Abela, T. E. Glover, P. A. Heimann, R. W. Schoenlein, S. L. Johnson, A. M. Lindenberg, and R. W. Falcone, Rev. Sci. Instrum. **75**, 24 (2004).
[43]C. M. Schlepuetz, R. Herger, P. R. Willmott, B. D. Patterson, O. Bunk, C. Broennimann, B. Henrich, G. Huelsen, and E. F. Eikenberry, Acta Crystallogr. Sect. A **61**, 418 (2005).
[44]S. L. Johnson, P. Beaud, C. J. Milne, F. S. Krasniqi, E. S. Zijlstra, M. E. Garcia, M. Kaiser, D. Grolimund, R. Abela, and G. Ingold, Phys. Rev. Lett. **100**, 155501 (2008).
[45]S. L. Johnson, P. Beaud, E. Vorobeva, C. J. Milne, D. Murray, S. Fahy, and G. Ingold, Acta Crystallogr. Sect. A **66**, 157 (2010).
[46]J. H. Jung, K. H. Kim, T. W. Noh, E. J. Choi, and J. Yu, Phys. Rev. B **57**, R11043 (1998).
[47]D. M. Fritz *et al.*, Science **315**, 633 (2007).
[48]K.-J. Jang, J. Lim, J. Ahn, J.-H. Kim, K.-J. Yee, and J. S. Ahn, Phys. Rev. B **81**, 214416 (2010).
[49]P. G. Radaelli, D. E. Cox, M. Marezio, and S.-W. Cheong, Phys. Rev. B **55**, 3015 (1997).
[50]G. C. Milward, M. J. Calderón, and P. B. Littlewood, Nature (London) **433**, 607 (2005).
[51]K. Ishioka and O. V. Misochko, *Progress in Ultrafast Intense Laser Science V*, edited by K. Yamanouchi, A. Giulietti, and K. Ledingham (Springer, Berlin, 2009), Vol. 98.
[52]H. J. Zeiger, J. Vidal, T. K. Cheng, E. P. Ippen, G. Dresselhaus, and M. S. Dresselhaus, Phys. Rev. B **45**, 768 (1992).
[53]S. Wall, D. Wegkamp, L. Foglia, K. Appavoo, J. Nag, R. F. Haglund, Jr., J. Stähler, and M. Wolf, Nat. Commun. **3**, 721 (2012).
[54]A. Cavalleri, T. Dekorsy, H. H. W. Chong, J. C. Kieffer, and R. W. Schoenlein, Phys. Rev. B **70**, 161102 (2004).
[55]V. A. Amelitchev, B. Güttler, O. Y. Gorbenko, A. R. Kaul, A. A. Bosak, and A. Y. Ganin, Phys. Rev. B **63**, 104430 (2001).